Applied Catalysis B: Environment and Energy 348 (2024) 123829

Contents lists available at ScienceDirect

Applied Catalysis B: Environment and Energy

journal homepage: www.elsevier.com/locate/apcatb

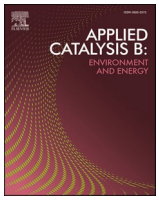

Tandemly coupled CO_2 hydrogenation and carbonylation on SiO_2-encapsulated Cu-ZnO nanoparticles with Ferrierite zeolite toward selective synthesis of oxygenates

Xu Wang, So Yun Jeong, Hyun Seung Jung, Jong Wook Bae *

School of Chemical Engineering, Sungkyunkwan University (SKKU), 2066 Seobu-ro, Jangan-gu, Suwon, Gyeonggi-do 16419, Republic of Korea

ARTICLE INFO

Keywords:
Tandem reaction
Encapsulated Cu-ZnO nanoparticles
Nano-sized Ferrierite (NFER)
CO_2 hydrogenation
Carbonylation
Thermally stable core-shell structures

ABSTRACT

Tandemly coupled gas-phase CO_2 hydrogenation reaction to dimethyl ether (DME) with its successive carbonylation (CO insertion) for one-step methyl acetate (MA) synthesis was investigated on newly designed SiO_2-encapsulated Cu-ZnO nanoparticles (CZ@Si) hybridized with nano-sized Ferrierite (NFER) zeolite. The core-shell-structured CZ@Si with thermally stabilized Cu-ZnO nanoparticles having stronger Cu-O-Si interfaces was crucial to form an optimal CO/DME ratio, which was found to be a key step to switch the reaction pathway from methanol-mediate hydrocarbon formation route to carbonylation route to selectively synthesize oxygenates by CO_2 hydrogenation-initiated tandemly coupled reaction. The formed methanol intermediate was further reacted to form DME by methanol dehydration, and the rates of surface methoxy formation and CO insertion to form acetyl intermediate were enhanced with the increased Brønsted acid sites in 8-membered ring channels on the NFER with higher MA selectivity of ~50% through novel tandem reaction for efficient CO_2 utilization.

1. Introduction

Tremendous efforts have been devoted over past decades to establish the methods of efficient carbon dioxide (CO_2) utilizations aimed at decreasing CO_2 emissions to achieve its net zero or negative emission. Among many recently reported technologies, selective reduction methods of CO_2 by hydrogenation offer an opportunity to produce sustainable fuels and petrochemicals. Liquid or gas-phase carbonylation reactions involving carbon-carbon coupling reaction (CO insertion) to increase carbon-chain numbers, which are one of the emerging and promising technologies to industrially manufacture bulk and fine petrochemicals, are usually employed with toxic CO molecule as C_1 feed source by various specialized synthetic methods [1–4]. The CO_2, as an abundant, nontoxic and recyclable C_1 source, has been widely used as CO surrogate for homogenous carbonylation reactions to produce acetic acid, higher carboxylic acids or ethanol [5–11]. The mixture of CO_2 and H_2 was engaged for a reverse water gas shift reaction (RWGS) to in-situ generate CO and successively participate in carbonylation reaction to attain final carbonylic products. In this pathway, CO_2 was used as C_1 feed source to substitute CO via RWGS reaction, and additional oxygenates such as ester and methanol were co-fed with CO_2/H_2 for one-step carbonylation reaction as well [5–7]. Besides, it has been well-recognized that CO_2/H_2 mixed gases can produce not only CO by RWGS reaction but also other lower alcohol (methanol) or ether (dimethyl ether, DME) on the well-developed methanol synthesis catalysts or hybridized with solid acid catalysts, respectively [12–16]. In addition, methanol-mediate pathway by using metal oxides (methanol/DME synthesis by CO_2 hydrogenation) combined with zeolite (Methanol/DME-to-hydrocarbons, D(M)TH) through tandem catalysis were well-established to efficiently synthesize higher hydrocarbons [15, 17]. However, it is difficult to selectively form oxygenates and still a challengeable task to be capable of simultaneously using CO and alcohol (methanol/DME) formed by RWGS reaction during CO_2 hydrogenation to achieve one-step tandemly coupled reactions for the selective synthesis of methyl acetate (MA) by suppressing the formation of light hydrocarbons through well-known methanol-mediate pathway.

The present study is to utilize CO_2 to form methanol/DME and CO simultaneously, and successive carbonylation of DME to form higher oxygenates such as methyl acetate and ethanol through tandemly coupled methanol-mediate pathway as schematically displayed in Scheme 1. The CO_2 hydrogenation to form methanol and RWGS reaction can be well-adjusted by using core-shell-structured Cu-ZnO@SiO_2 (CZ@Si) catalyst with its higher thermal stability, which can form an appropriate CO/methanol ratio (step (1) and (2)). The formed methanol

* Corresponding author.
E-mail address: finejw@skku.edu (J.W. Bae).

https://doi.org/10.1016/j.apcatb.2024.123829
Received 11 November 2023; Received in revised form 31 January 2024; Accepted 6 February 2024
Available online 10 February 2024

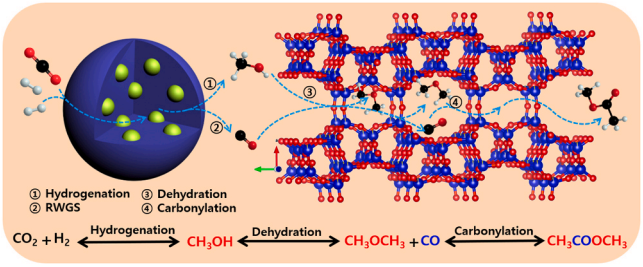

Scheme 1. Schematic diagram of tandemly coupled RWGS/methanol synthesis reaction with in-situ carbonylation of CO/DME for direct methyl acetate synthesis by CO_2 hydrogenation.

intermediate can be diffused into FER zeolite micropores to engage in its dehydration to form DME intermediate (step (3)), which is further carbonylated with CO in 8-membered ring (8-MR) channels of FER zeolite to eventually synthesize MA product (step (4)). Since the RWGS reaction has strong endothermic nature, which is favourable under higher temperatures [12], while the highly exothermic methanol/DME carbonylation is more favourable at lower temperatures from thermodynamic considerations (supplementary Fig. S1). Therefore, a higher reaction temperature will trigger undesirable side reactions such as methanol-to-hydrocarbon (MTH) or DME-to-hydrocarbon (DTH) during the gas-phase carbonylation by forming lots of byproducts. To successfully achieve the tandemly coupled RWGS, CO_2 hydrogenation and its successive carbonylation with an in-situ formed CO and DME by directly using CO-CO_2-H_2 containing syngas, the optimal reaction conditions and stable hybrid catalysts should be considered to obtain higher RWGS activity as well as to adjust CO_2 hydrogenation activity for higher successive carbonylation activity by using proper ratio of CO/DME feed. Eventually, we succeeded in coupling the tandem reactions to achieve one-step MA synthesis from CO_2 hydrogenation on the hybridized tandem catalyst, which proposed a new approach for the selective synthesis of C_2^+ oxygenates directly from CO/CO_2 mixtures without any additional complicated separation processes of syngas into CO, CO_2 and H_2 separately.

Compared to the well-known CO_2 hydrogenation to higher hydrocarbons through methanol-mediate pathway [15,17], the present direct synthesis of MA oxygenate through successive CO_2 hydrogenation-dehydration-carbonylation on the tandemly coupled Cu-ZnO@SiO_2/FER also suggested the possibility of direct utilization of CO_2 to produce value-added oxygenates. The types of metal oxides for CO_2 hydrogenation to methanol and RWGS reaction to form CO and zeolite topologies for dehydration of methanol to DME with its successive carbonylation to MA on acidic sites of various zeolites [18,19] have been investigated briefly with the effects of their proximity. It eventually suggests an efficient novel hybridizing method to prepare thermally stable and catalytic active systems by introducing the homogeneously dispersed Cu-ZnO nanoparticles encapsulated with SiO_2 overlayers (~20 nm in size), which was further tandemly hybridized with specific nano-sized FER having the particle size of ~200 nm as an excellent catalyst for methanol dehydration and DME carbonylation simultaneously.

2. Experimental section

2.1. Catalyst preparation

SiO_2-encapsulated Cu-ZnO nanoparticles (~3 nm in size) were prepared by the well-known reverse micelle method with copper and zinc metal precursors, where Cu/Zn mole ratio was varied by changing its mole ratio with 3/7, 5/5, 7/3 and 10/0. Typical Cu-ZnO-Al_2O_3 (denoted as CZA) was prepared by co-precipitation method. The $ZnZrO_x$ metal oxides were prepared by the conventional coprecipitation method and the nanostructured FER zeolite (NFER) was also synthesized by a typical hydrothermal synthesis method. The nanosheet-structured FER zeolite (NSFER) was prepared with using organic structure directing agent (OSDA) and organic soft template to synthesize specific thin-layer morphology with its higher crystallinity. The H-form commercial FER (CFER) was purchased from Vision Chem. and NH_4-form Mordenite was bought from Alfa Aesar and transformed to H-form MOR (CMOR), and the dealuminated CMOR (DCMOR) in the 12-membered ring (12-MR) channels was also prepared as a reference zeolite. The hybridized CZ@Si/HZSM-5 and CZ@Si/NFER for CO_2 hydrogenation to DME (as well as methanol) were prepared by simple powder mixing method with different weight ratio of CZ@Si and zeolite (HZSM-5 and NFER). The more detailed preparation methods are included in supplementary material.

2.2. Characterization and activity measurement

The textual properties were measured by N_2 adsorption-desorption analysis and powder X-ray diffraction (XRD) analysis was used to verify crystalline structures with the help of transmission electron microscopy (TEM) analysis. Temperature-programmed reduction (TPR), temperature-programmed desorption of NH_3 (NH_3-TPD) and temperature-programmed desorption of CO_2 and H_2O (TPD) analysis were performed, and Fourier-Transform infrared spectroscopy (FT-IR) and Diffuse Reflectance Infrared Fourier Transform Spectroscopy (DRIFTS) analysis were carried out to verify surface properties. The catalytic activity for direct MA formation by gas-phase CO_2 hydrogenation was evaluated with 0.2 g metal oxide and different amounts of zeolites by using a gas chromatography (GC, YL6100, Younglin). The more detailed experimental procedures are included in supplementary material.

3. Results and discussion

3.1. Catalyst properties and performances on metal oxides

CO_2 conversion to methanol by CO_2 hydrogenation with its exothermic nature and RWGS reaction to form CO with its endothermic nature are thermodynamically competitive reactions (supplementary Fig. S1**(A)**), where the exothermic CO_2 hydrogenation activity to methanol is limited by thermodynamic equilibrium [12]. In terms of the selective oxygenates formations through CO_2 hydrogenation, the RWGS reaction activity seems to be expected to be suppressed because the formed CO byproduct decreases the oxygenates selectivity [12–14]. Therefore, many modified Cu-ZnO-Al_2O_3 (CZA) catalysts have been investigated to boost up methanol selectivity by suppressing the RWGS activity [14,20], where the RWGS reaction to form CO on the Cu-based catalysts is inevitable and thermodynamically more feasible at higher temperatures. Therefore, some non-copper-based catalysts with various metal oxides such as ZnO-ZrO_2 or In_2O_3 have been largely investigated to obtain comparable CO_2 conversion to methanol with an extremely lower RWGS reaction activity [21–26]. In addition, the RWGS reaction at higher temperatures is found to be more thermodynamically favorable, and the higher temperatures are also favorable for preferential formations of undesired byproducts (mainly C_1 - C_3 hydrocarbons) as displayed in supplementary Fig. S1**(B)**. For the present novel tandem reactions of CO_2 hydrogenation-dehydration-carbonylation, the in-situ formed CO molecules act as a crucial intermediate with methanol or DME to form MA product through a direct carbonylation reaction, which can be well realized on the thermally stable CZ@Si hybridized with an optimal FER zeolite.

Therefore, three different general methanol synthesis catalysts such as $ZnZrO_x$, Cu-ZnO-Al_2O_3 (CZA) and core-shell structured CZ@Si were separately compared to elucidate the effects of formed CO/DME ratio to its successive gas-phase carbonylation to MA by CO_2 hydrogenation and RWGS reaction, which have their respective surface areas of 48, 41 and

102 m^2/g with typical mesoporous structures and larger intra-particular pores (supplementary Table S1 and Fig. S2). As shown in Fig. 1**(A)** and supplementary Fig. S3, the multicore-structured Cu-ZnO nanoparticles with its homogeneous size distribution of ~3 nm (CuO content of 4.41 wt% and 1.86 wt%ZnO as shown in Table S1) were well encapsulated with SiO_2 overlayer shells, which has its nanosphere size of ~30 nm and pore diameter of 15.4 nm mainly originated from the intra-particular pores (no characteristic crystalline peaks of SiO_2 as shown in Fig. 1**(D)**). The well-dispersed and spatially confined Cu-ZnO nanoparticles with larger pore volume of 0.38 cm^3/g and thicker SiO_2 shells revealed their much higher thermal resistances with smaller aggregation characteristics. However, the Cu-ZnO-Al_2O_3 (CZA) catalyst showed the largely aggregated morphology of the main CuO(−111) phases with its characteristic lattice parameter of 0.253 nm with its characteristic XRD patterns as shown in Fig. 1**(B)** and 1**(D)**. The $ZnZrO_x$ metal oxides possessing 8.1 wt%ZnO showed the bulk ZrO_2(011) phases with its characteristic lattice parameter of 0.295 nm and no clear observations of the crystalline ZnO phases were found due to its highly dispersed natures as shown in Fig. 1**(C)** and 1**(D)**.

Based on H_2-TPR results as displayed in Fig. 1**(E)** and summarized in supplementary Table S1, CuO phases on the CZA were easily reduced with its maximum peak temperature of 259 °C compared to that of 268 °C on the CZ@Si with a larger H_2 uptake of 4.931 mmol/g on the CZA compared to that of 1.116 mmol/g on the CZ@Si measured in the temperature range of 100 – 400 °C. Those observations were mainly attributed to the SiO_2 encapsulation-induced strong interactions between CuO and SiO_2 shells by forming Cu-O-Si interfaces as supported by larger peak intensity at 613 °C (H_2 uptakes of 0.761 mmol/g) on the CZ@Si compared to the CZA. The shoulder peak at 331 °C on the CZA was originated from the heterogenous distributions of the CuO

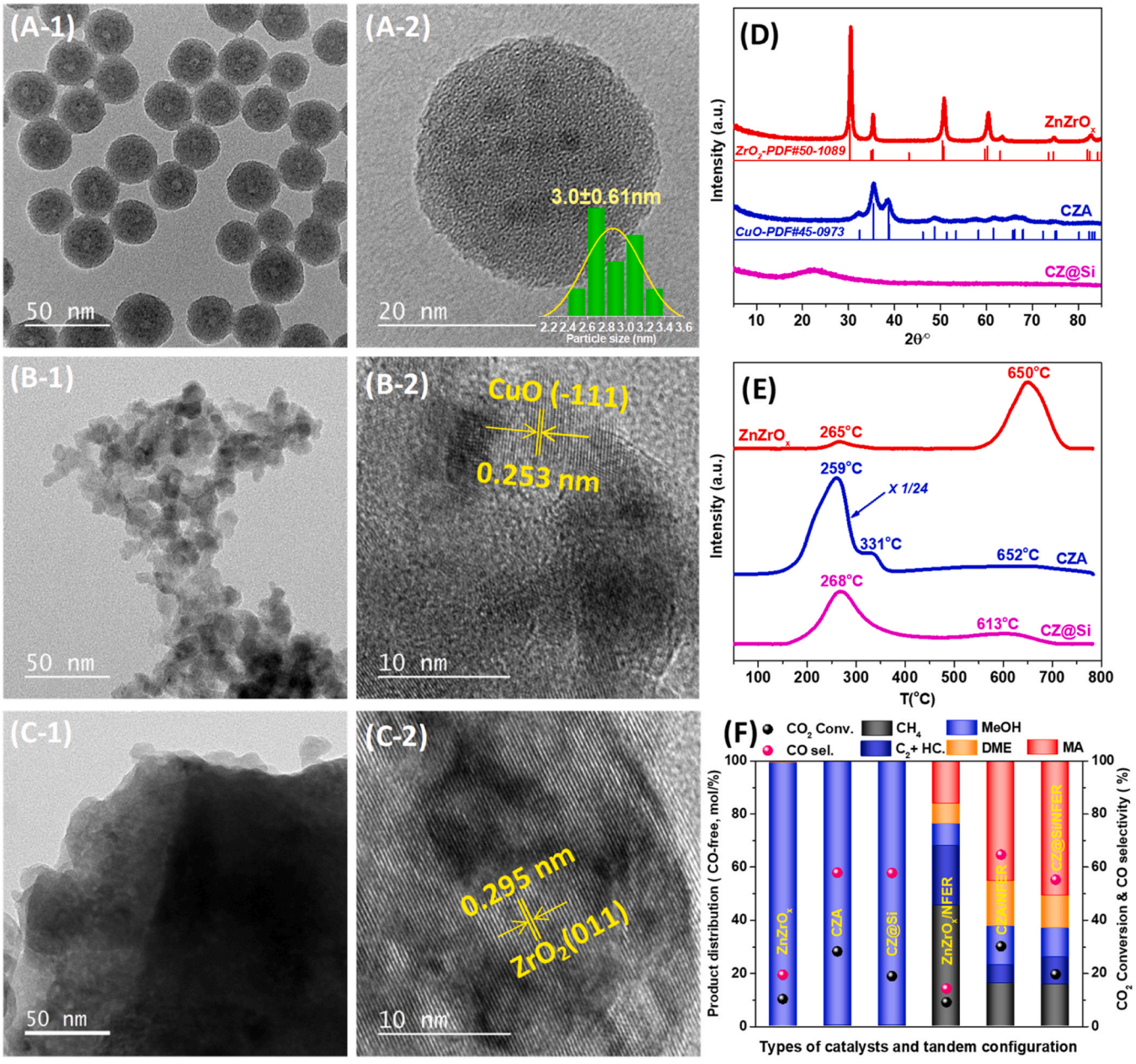

Fig. 1. Catalytic performances and characterization results on the separate fresh metal oxides; **(A)** HRTEM images of CZ@Si, **(B)** HRTEM images of CZA, **(C)** HRTEM images of ZnZrOx, **(D)** XRD patterns, **(E)** TPR patterns and (**F**) Catalytic activity on the metal oxide catalyst itself (ZnZrOx, CZA and CZ@Si) and tandem catalytic system with distinctive metal oxides/NFER for direct CO_2 hydrogenation to MA under the reaction condition of T = 300 °C, P = 5.0 MPa, H_2/CO_2 molar ratio = 3 (4 vol% N_2 balanced) and space velocity (SV) = 625 mL/(g_{cat}·h).

nanoparticles by forming the much stronger interactions in the Cu-ZnO-Al_2O_3 matrices. In addition, the larger reduction peak of 650 °C on the $ZnZrO_x$ was attributed to the reduction of ZnO or ZrO_2 due to the possible formation of solid solutions [26] and smaller reduction peak at 265 °C for partial reductions of ZnO particles [27] with their respective H_2 uptakes of 0.008 and 1.287 mmol/g. In addition, CO_2-TPD results revealed that the CO_2 absorption capability below 300 °C was found in the following order of $ZnZrO_x$ > CZA > CZ@Si in the range of 0.04 – 0.33 mmol/g as summarized in supplementary Fig. S4 and Table S1. The larger amount of the adsorbed CO_2 on the $ZnZrO_x$ was attributed to its larger oxygen vacant sites [27], and larger H_2 uptakes and smaller CO_2 uptakes was originated from a relatively difficult reducibility of CuO phases on the CZ@Si, which are responsible for facile light hydrocarbons formations.

Catalytic activity for CO_2 hydrogenation to methanol and CO formed by RWGS reaction on the $ZnZrO_x$, CZA, CZ@Si are shown in Fig. 1**(F)** and supplementary Table S2. In general, an increase of reaction temperature enhances CO selectivity due to thermodynamically favorable RWGS reaction nature, especially on the CZA having larger metallic Cu sites (66.1 wt%CuO, 28.9 wt%ZnO and 5.0 wt%Al_2O_3) with its smaller activation energy (Ea) of 32.4 kJ/mol. However, larger Ea values of 80.6 and 90.9 kJ/mol on the CZ@Si and $ZnZrO_x$ were attributed to the difficult activations of CO_2 by limited mass transfer rate through the porous SiO_2 shells with smaller Cu active sites (4.41% CuO, 1.86 wt% ZnO and 93.73 wt% SiO_2) and the smaller active oxygen vacant sites on the $ZnZrO_x$ were also responsible for its lower activity for CO_2 hydrogenation and RWGS reaction. The much higher CO_2 conversions in the range of 26.2 – 29.5% and higher CO selectivity in the range of 39.0 – 72.9% in the temperature range of 250–310 °C were observed on the CZA compared to the $ZnZrO_x$ (CO_2 conversion in the range of 4.1 – 11.6%), which were mainly attributed to the largely exposed metallic Cu surfaces. As summarized in supplementary Table S3 (measured at T = 300 °C and space velocity (SV) = 625 mL/(g_{cat}·h)), the higher CO_2 conversion of 28.3% as well as higher selectivity to CO with 57.9% and lower CH_4 selectivity of 0.4% on the CZA were observed due to its larger active metallic Cu sites compared to the CZ@Si with lower CO_2 conversion of 19.0% and similar CO selectivity of 57.8% as well as $ZnZrO_x$ with a little lower CO_2 conversion of 10.4% and much lower CO selectivity of 19.5%.

Apparently, the higher RWGS activity and proper CO_2 hydrogenation to methanol (or DME) with higher CO/DME ratio are crucial to enlarger the carbonylation activity and to suppress the formation of hydrocarbons through methanol-mediate pathway, and the CZ@Si with higher CO selectivity and lower methanol yield compared to the CZA and $ZnZrO_x$ seems to be more proper for further successive reaction such as tandemly coupled gas-phase carbonylation reaction. Therefore, the CZ@Si coupled with nanosized-FER zeolite (NFER) also revealed the higher tandemly coupled reaction activity for a direct synthesis of MA by CO_2 hydrogenation with smaller hydrocarbon formation. The highest MA selectivity of 50.8% (MA productivity of 328.8 g/(kg_{cat}·h)) was observed on the CZ@Si/NFER with CO_2 conversion of 19.7% and relatively higher light hydrocarbons selectivity of 26.0% at 300 °C, which

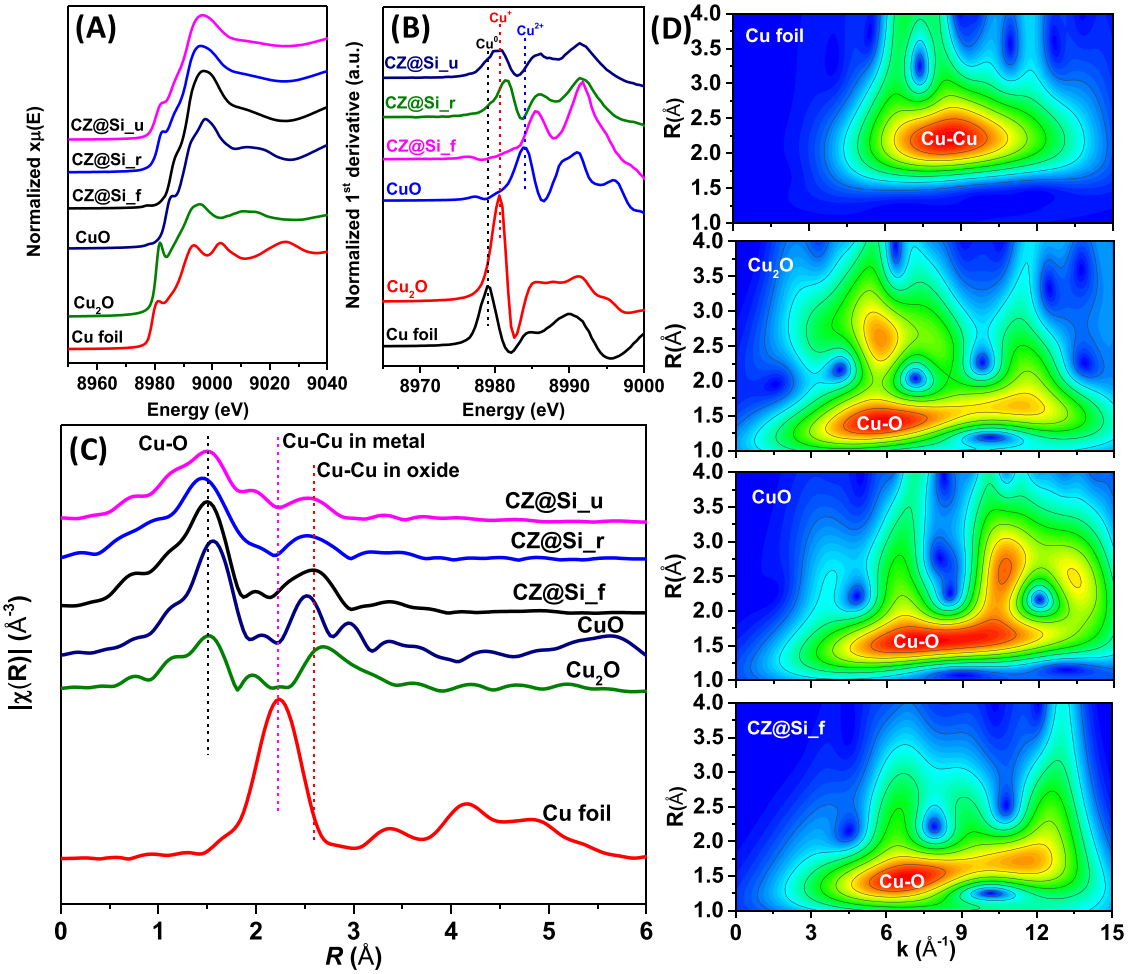

Fig. 2. Local structures and electronic properties of Cu-ZnO nanoparticles in the CZ@Si; **(A)** Normalized Cu K-edge XANES spectra, **(B)** Normalized 1st derivative of Cu K-edge XANES spectra, **(C)** Fourier transformations in R-space and **(D)** Wavelet transform (WT) of Cu foil, Cu_2O, CuO and fresh CZ@Si (CZ@Si_f), reduced CZ@Si (CZ@Si_r) and used CZ@Si (CZ@Si_u) catalyst.

were attributed to the increased thermal stability of the core-shell structured CZ@Si with smaller CO_2 uptakes by preserving its original crystallite size and morphology as displayed in supplementary Fig. S5. To further confirm the chemical oxidation states of the CZ@Si catalyst, X-ray absorption fine spectroscopy (XAFS) analysis of the Cu K-edge was carried out and the results are displayed in Fig. 2. It is also displayed in Fig. 2**(A)** with the normalized absorbance X-ray absorption near edge spectra (XANES) and the normalized first derivative spectra of the CZ@Si in Fig. 2**(B)**, where the copper oxidation states were mainly in the form of Cu^{2+} species in the fresh CZ@Si catalyst while it was reduced to Cu^{+} species with strong metal support interaction (SMSI) by forming Cu-O-Si interfaces [28]. The presence of SiO_2 shells was to stabilize the Cu^0/Cu^+ phases due to the SMSI effects between Cu and SiO_2 shells as shown in Fig. 2**(C)** and Fig. 2**(D)**, where the simulated coordination environments of those Cu species strongly suggested the possible existence of Cu-O-Si interfaces on the used CZ@Si catalyst.

In addition, it was also found to be similar on the CZA/NFER with higher CO_2 conversion of 30.2% and MA selectivity of 45.3%, however the lower CO_2 conversion of 9.2% and MA selectivity of 16.1% were observed on the $ZnZrO_x$/NFER as summarized in supplementary Table S3. Those observations were attributed to the lower CO/DME ratio of 0.9 on the $ZnZrO_x$/NFER compared to the CZ@Si/NFER with that of 5.0 due to the suppressed RWGS reaction activity. The relatively lower MA selectivity on the CZA/NFER even with the highest CO/DME ratio of 5.6 seems to be attributed to fast competitive adsorption natures of the water on the NFER surfaces formed by methanol dehydration compared to the CZ@Si/NFER, which suggests that an optimal CO/DME ratio from CO_2 hydrogenation and RWGS reaction and surface hydrophobicity to easily remove adsorbed water are also crucial for enhancing activity.

3.2. Catalyst property and activity of CZ@Si hybridized with different zeolites

The thermally stable core-shell-structured CZ@Si showing a proper RWGS activity to form CO and methanol was selected to further confirm in-situ carbonylation activity according to different morphology of various zeolites [26–34] such as dealuminated commercial MOR in the 12-membered ring (12-MR) channels (DCMOR), commercial FER (CFER), nanosheet-structured FER (NSFER) and nano-sized FER (NFER) containing 8-membered ring (8-MR) channels. Those zeolites are to enhance the carbonylation activity on the active sites in the 8-MR channels to suppress hydrocarbon formations and to increase MA oxygenate selectivity. The bulk Si/Al ratios on those zeolites measured by XRF analysis were found in the range of 10.2 – 12.9 with the largest ratio on the NSFER as summarized in Table 1 and supplementary Table S4. The specific surface area, pore volume and average pore diameter were found to be larger on the NSFER among the other FERs with the respective value of 340.6 m^2/g, 0.44 cm^3/g and 16.2 nm, which were attributed to its nanosheet-like structure with larger intra-particular mesopores and typical type IV isotherm as shown in supplementary Fig. S6**(A)** and **6(B)**. On the NFER, the surface area of 299.8 m^2/g and average pore diameter of 4.3 nm were observed, which were attributed to the intra-particles mesopores between nano-structured NFER crystallites. As displayed in Fig. 3, the DCMOR (largest surface area of 371.1 m^2/g) and CFER showed their distinctive morphology such as micro-sized crystallites (Fig. 3**(A)** and 3**(B)**). In addition, the NSFER and NFER showed the sheet-like aggregated crystallites with the entangled stripe shapes (Fig. 3**(C)**) and nano-sized crystallites with ~ 200 nm in size (Fig. 3**(D)**), which are well in line with the XRD results as shown in supplementary Fig. S6**(C)**.

The surface acidic sites on the different zeolites were measured by NH_3-TPD and Py-IR analysis and the results are displayed in Fig. 3**(E)** as well as Fig. 4**(A)** and summarized in Table 1. The stronger acidic sites on the DCMOR (0.391 mmol/g) assigned to the peak at 515 °C (total acidic sites with 1.181 mmol/g) were found to be much smaller than that of the NFER (0.490 mmol/g) and higher than CFER (0.290 mmol/g) with the smallest total acidic sites of 0.879 mmol/g on the NSFER, which suggests that the much stronger acidic sites on the DCMOR (515 °C) compared to other FERs (420 – 460 °C) were responsible for the selective formations of larger amount of hydrocarbons. The larger amount of

Table 1
Bulk and surface properties of the fresh zeolite and catalytic activity of the hybridized CZ@Si and zeolite tandem catalyst.

Zeolite	XRF[a]	N_2–sorption[b]			NH_3-TPD[c]	Py-IR[d]	H_2O-TPD[e]	Acidic site (8-MR)[f] (mmol/g)	X_{CO2} (%)	S_{CO} (%)	CO-free selectivity (%)[g]
	Si/Al ratio	S_g (m^2/g)	P_V (cm^3/g)	P_D (nm)	W/M/S (total) (mmol/g)	B/L	D_{H2O}				C_1/C_{2+}/methanol/DME/MA
NFER	11.5	299.8	0.19	4.3	0.464/0.235/0.490 (1.189)	0.232/0.019	0.92	0.258	19.7	55.3	15.7/10.3/11.0/12.2/50.8
NSFER	12.9	340.6	0.44	16.2	0.357/0.228/0.294 (0.879)	0.102/0.011	0.66	0.192	20.2	69.9	8.6/6.1/22.2/21.6/41.5
CFER	10.6	272.6	0.12	3.7	0.631/0.309/0.290 (1.230)	0.095/0.003	1.00	0.195	19.3	69.3	45.1/32.0/0.0/1.6/21.3
DCMOR	19.8	371.1	0.08	9.4	0.692/0.098/0.391(1.181)	0.286/0.018	0.38	0.105	18.4	54.6	21.4/68.7/9.9/0/0

[a] Si/Al molar ratios on the fresh zeolites were determined by XRF analysis, where the NSFER, NSFER, CFER and DCMOR represents the nanostructured FER, nanosheet FER, commercial sphere-type FER zeolite, commercial Mordenite and dealuminated commercial Mordenite in 12-membered ring (12-MR) channels, respectively.

[b] Specific surface area (S_g, m^2/g), pore volume (P_V, cm^3/g) and average pore diameter (P_D, nm) were characterized by N_2 adsorption-desorption analysis on the fresh zeolites.

[c] Acidic sites on the fresh zeolites were measured by NH_3-TPD analysis, and the amounts of weak (W), medium (M) and strong (S) acid sites were calculated with an integrated area at maximum desorption temperature of NH_3 at 208–216 °C, 336–365 °C and 455–490 °C, respectively.

[d] Amounts of Brønsted (B) and Lewis (L) acid sites were measured by pyridine FT-IR (Py-IR) at the adsorption temperature of 250 °C, and the number of acidic sites (mmol/g) were calculated by using the formula of B sites = $1.88A_BR^2/W$, L sites = $1.42A_LR^2/W$, where A_B and A_L stand for the integrated absorbance peak area of Brønsted and Lewis acid sites appeared at 1550 and 1450 cm^{-1}, respectively.

[e] D_{H2O} represents the relative surface hydrophobicity based on the CFER by calculating the desorption peak area ratio at a higher temperature (190–200 °C) based on the area of the CFER zeolite.

[f] Amounts of Brønsted acid sites in the 8-membered ring (8-MR) channels in the zeolites were calculated by using the equation of [overall number of Brønsted acid sites (strong acid sites from NH_3-TPD) – number of Brønsted acid sites in the 10-MR channels (Py-IR analysis)].

[g] Catalytic activity such as CO_2 conversion (X_{CO2}), CO_2 conversion to CO (S_{CO}) and CO-free selectivity on the various CZ@Si-hybridized zeolites (0.2 g CZ@Si and 1.4 g each zeolite) was represented with a steady-state value measured at T = 300 °C, P = 5.0 MPa, space velocity (SV) = 625 mL/(g_{cat}·h) and a feed gas composition of $CO_2/H_2/N_2$ = 72/24/4, where the catalyst was previously reduced at 300 °C for 2 h under a flow of 5 vol%H_2 balanced with N_2.

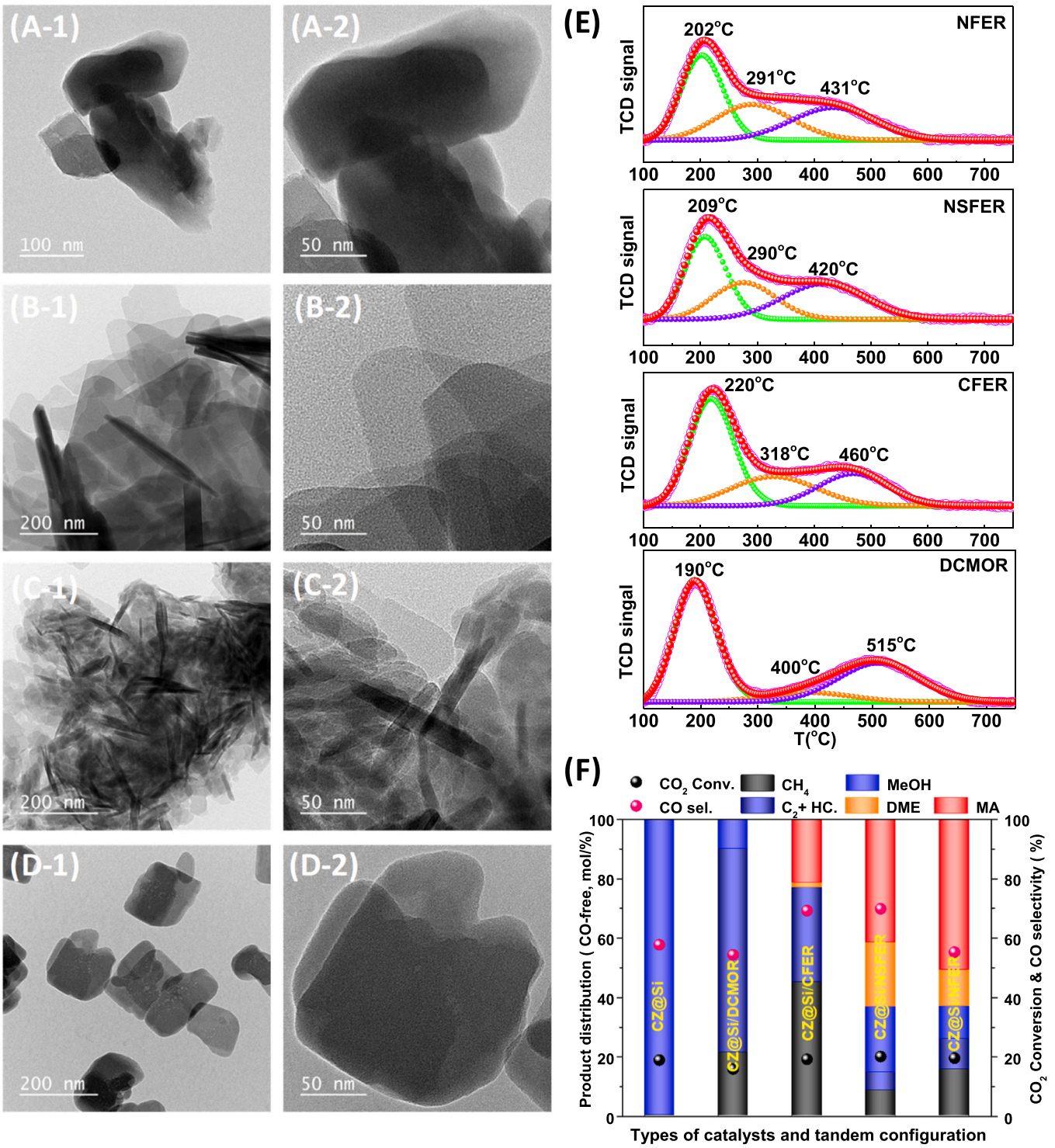

Fig. 3. Catalytic performances and characterization results of four different zeolites; **(A)** HRTEM images of the dealuminated DCMOR, **(B)** HRTEM images of the commercial FER zeolite (CFER), **(C)** HRTEM images of the nanosheet-FER (NSFER), **(D)** HRTEM images of the nano-sized FER (NFER), **(E)** Temperature-programed desorption of NH_3 (NH_3-TPD) on different zeolites and **(F)** Catalytic performances on the CZ@Si and hybridized CZ@Si/zeolite for CO_2 hydrogenation to MA under the reaction conditions of T = 300 °C, P = 5.0 MPa, H_2/CO_2 = 3 (with 4 vol%N_2 balanced) and SV = 625 mL/(g_{cat}·h).

Brønsted (B) acid sites (0.232 mmol/g) on the NFER measured by Py-IR analysis were also responsible for the enhanced carbonylation activity with the decreased hydrocarbons formations. In addition, the coke formations measured by TGA were found to be smaller on the used DCMOR and slightly higher on the used NFER compared to the CFER as shown in Fig. 4**(B)**, which were attributed to the decreased Brønsted (B) acid sites in the 12-MR channels by suppressing coke depositions and heavy hydrocarbon formations to enhance catalyst stability as well as by increasing fast CO insertion rate to selectively form MA product via acetyl intermediate [33,35] instead of the formation of coke precursors on the strong Brønsted (B) acid sites in the 8-MR channels of the NFER zeolite. Furthermore, the much lower DME desorption temperature of 252 °C on the DCMOR (DME-TPD analysis as shown in Fig. 4**(C)**) was responsible for an easier dissociation of DME molecules on the much

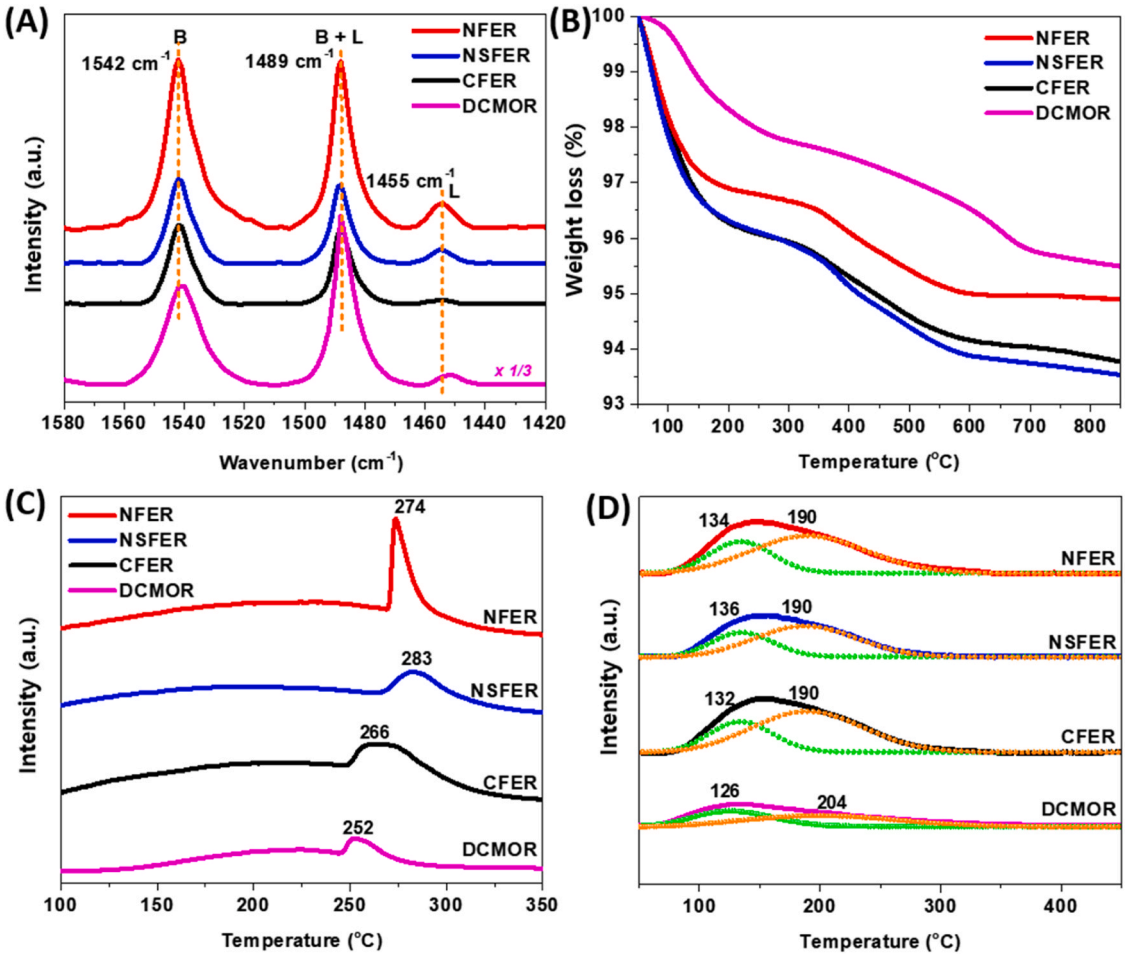

Fig. 4. Surface properties on the various zeolites; **(A)** Pyridine-IR spectra, **(B)** TGA profiles of the used zeolites, **(C)** DME-TPD and **(D)** H_2O-TPD profiles.

stronger acidic sites to selectively form hydrocarbons, which was also found to be much higher on the NFER and NSFER in the range of 274 – 283 °C. The higher desorption temperature and larger intensity on the NFER were responsible for the enhanced carbonylation activity through the formations of stably dissociated DME molecules on the acidic sites. In addition, the desorption temperature of water (H_2O-TPD analysis) as displayed in Fig. 4**(D)** and summarized in Table 1 revealed that the DCMOR was found to have more hydrophobic surfaces with the lowest relative water adsorption capacity (D_{H2O}) with 0.38 compared to the reference CFER (1.0). The lower respective values of 0.92 and 0.66 on the NFER and NSFER can enhance the carbonylation activity by increasing CO adsorption rate due to the suppressed competitive adsorption of water on the active Brønsted acid sites [19,29]. The characteristics of hydrophobic surfaces with smaller water desorption capacity were found to be in the order of DCMOR >> NFER ≅ NSFER > CFER, which were well-related with MA selectivity due to the adjusted water adsorption formed by RWGS reaction in the FERs. The DCMOR was found to have most hydrophobic surfaces with no MA formation, which was attributed to the presence of much stronger Brønsted acid sites in the 8-MR channels of the DCMOR (even after the selective removal of Brønsted acid sites in the 12-MR channels of the CMOR by dealumination as shown in supplementary Fig. S6**(D)**) by enhancing the D/MTH reaction activity instead of carbonylation reaction for oxygenates at 300 °C as confirmed by DME carbonylation activity to selectively form hydrocarbons at higher reaction temperature. Therefore, the larger amount of Brønsted acid sites in the 8-MR channels with 0.258 mmol/g on the NFER compared to that of 0.195 mmol/g on the CFER was responsible for the enhanced carbonylation activity [29,33,35], where the larger amount of much stronger total acidic sites (1.181 mmol/g) with its smaller Brønsted acid sites in the 8-MR channels of 0.105 mmol/g on the DCMOR even with its more hydrophobic surface natures seems to be responsible for the selective formations of light hydrocarbons as summarized in Table 1.

Based on the natures of the different zeolites, catalytic activity and product distribution on the hybridized CZ@Si/zeolites are summarized in Table 1 and supplementary Table S4 as well as displayed in Fig. 3**(F)**. The CZ@Si itself showed the higher RWGS activity with CO selectivity of 57.8% at CO_2 conversion of 19.7% and 99.6% methanol selectivity with small amount of CH_4 at 300 °C and 5 MPa. The product distribution was largely changed after hybridizing the CZ@Si with various zeolites with similar CO_2 conversions in the range of 16.0 – 20.2%. On the CZ@Si/DCMOR, only paraffinic hydrocarbons were formed with a lower CO_2 conversion of 18.4% and larger C_{2+} hydrocarbons with 68.7% (lower CO_2 conversion to CO with 54.6% by RWGS reaction). These observations were attributed to the suppressed RWGS activity as well as possible methanol/DME reforming reactions to form hydrocarbons [36] on the much stronger abundant acidic sites with smaller Brønsted acid sites in the 8-MR channels of the DCMOR. A considerable MA selectivity of 21.3% at CO_2 conversion of 19.3% was observed with higher hydrocarbons selectivity of 77.1% (higher CO_2 conversion to CO with 69.3%), which suggests that the CZ@Si/CFER seems to selectively produce hydrocarbons through the present tandem reactions due to smaller Brønsted acid sites in the 8-MR channels and relatively hydrophilic surface natures. A higher selectivity to oxygenates was found on the CZ@Si/NFER with 74.0% (50.8% MA selectivity) at CO_2 conversion of 20.2%, and a relatively excellent MA selectivity of 41.5% was also

observed on the CZ@Si/NSFER, where the NFER zeolite has the largest Brønsted acid sites in the 8-MR channels (0.258 mmol/g) with more hydrophobic surface natures as well as proper CO/DME ratio of 5.0 (DME selectivity of 12.2% resulted in a higher MA productivity of 328.3 g/(kg_{cat}·h)), which seems to be proper for tandemly coupled reaction to produce value-added petrochemicals from CO_2 hydrogenation [36].

3.3. Optimization of CZ@Si/NFER and product distributions

To optimize the tandemly coupled catalytic reaction on the hybridized CZ@Si/zeolites for one-step MA synthesis by CO_2 hydrogenation, the effects of weight ratios of CZ@Si to NFER, catalyst-bed configurations, first layer compositions, Cu/Zn molar ratios on the CZ@Si and long-term stability on the CZ@Si/NFER were also investigated, and the results are displayed in Fig. 5. As displayed in Fig. 5**(A)** and summarized in supplementary Table S2, the CZ@Si catalyst itself showed the simple products distribution such as methanol and CO formed by RWGS reaction, and product distribution including MA was largely altered on the hybridized CZ@Si/NFER. The weight ratio of CZ@Si to NFER with 1/7 revealed a higher MA selectivity above 50.8% at CO_2 conversion of 20% compared to the weight ratio of 1/3 (main product of methanol), which strongly suggests the crucial contributions of the NFER zeolite for methanol dehydration as well as DME carbonylation to MA. Those tandemly coupled catalytic reactions on the hybridized catalysts generally showed largely different catalytic activity and product distribution due to the different proximity of two active sites and intimate proximity-derived detrimental effects [37–42]. Therefore, the different catalyst-bed configuration such as physical mixing (PM), granule mixing (GM) and dual-bed (DB) with the CZ@Si and NFER as schematically was displayed in supplementary Fig. S7 and further investigated and the typical results are displayed in Fig. 5**(B)** and supplementary Table S5. The physical and granule mixing configuration of the CZ@Si and NFER (PM and GM) revealed no significant MA formation compared to the appropriate DB configuration with 50.8% MA selectivity with a lower CO_2 conversion of 19.7%. The main byproducts of C_{2+} hydrocarbons and methanol on the PM and GM configuration (respective selectivity of 48.8 – 39.9% and 37.0 – 45.6%) were mainly attributed to the enhanced hydrogenation activity of the surface intermediates to form hydrocarbons (with relatively higher CO_2 conversion in the range of 23.9 – 24.1%) with lower dehydration activity due to the adsorption of excess water on the active Brønsted acid sites. In general, an intimate proximity for the tandemly coupled catalytic reaction system can boost up an intermediate diffusion rate, and it can change equilibriums for the adsorption and diffusion of intermediates. Furthermore, the different proximity of metal oxides with zeolites can change the local diffusion kinetics of intermediates (methanol/DME/CO) [42], which can significantly change product distributions due to the adjusted distances between metal oxides and zeolites. For the PM and GM configuration as shown in Fig. 5**(B)**, the much closer proximity induced the higher local methanol/DME concentration on the NFER zeolites as well as higher local CO concentration on the CZ@Si. Therefore, the gas-phase carbonylation activity on the NFER seems to be probably prohibited with significant MTH reaction activity to form hydrocarbons under excess methanol/DME environment. In addition, the formed methyl acetate can further proceed to hydrocarbons by fast hydrogenation due to the close contact between zeolites and active CZ@Si sites, where the formation of hydrocarbons can be also caused by the excess methanol/DME at its lower carbonylation activity under lower CO partial pressure. In addition, too close proximity usually leads to possible metal ion migrations to zeolites on the bifunctional catalysts [37], which can neutralize the surface acidic sites resulted in enhancing undesired reaction pathway to form byproducts as well. Therefore, the proximity effects on the product distributions for tandemly coupled catalytic reaction not only adjust diffusion kinetics but also change the interactions between metal oxides and zeolites resulted in changing catalytic activity and stability. The DB configuration with a far distance between two active sites with insignificant migrations of metal ions on zeolite surfaces [27,37] can further change methanol formation rate and its dehydration rate to DME as well as its carbonylation reaction to MA, which suppress the undesired side reactions such as hydrogenation of surface intermediates formed from methanol and DME adsorption.

For DME carbonylation on the hybridized catalysts, the surface concentration of CO and DME formed by RWGS reaction and CO_2 hydrogenation-dehydration are crucial for their successive gas-phase carbonylation on the NFER, where the surface DME concentration can be further adjusted by introducing the hybridized CZ@Si with solid acid zeolites such as FER and HZSM-5 with their different weight ratios. As displayed in Fig. 5**(C)** and summarized in supplementary Table S6, methanol selectivity was increased with an increase of weight of dehydration catalyst such as the HZSM-5 or FER zeolite in the first catalyst-layer due to thermodynamically favorable DME hydration with an excess amount of water formed by CO_2 hydrogenation to hydrocarbons, which inhibited DME carbonylation activity on the Brønsted acid sites (for example, higher MA productivity of 328.3 g/(kg_{cat}·h) on the CZ@Si/NFER and lower MA productivity of 140.1 g/(kg_{cat}·h) on the modified CZ@Si/NFER(2/1)/NFER). On the CZ@Si/HZSM-5(2/1) and CZ@Si/NFER(2/1) hybridized with the NFER zeolite, methanol selectivity was dramatically increased up to 40.8 – 55.9% with higher CO_2 conversions to CO in the range of 66.2 – 68.4% at similar CO_2 conversions of 18.1 – 21.2%. The selectivity to methanol was found to be much lower on the CZ@Si/NFER with its selectivity of 11.0% and CO_2 conversion to CO of 55.3% (at CO_2 conversion of 19.7%), which was also attributed to the appropriate surface CO/DME ratio of 5.0 to selectively form MA product as summarized in supplementary Table S6. In addition, the Cu/Zn molar ratios on the CZ@Si also played important roles by adjusting RWGS activity and methanol selectivity. Therefore, the effects of Cu/Zn ratios were further verified for the direct CO_2 hydrogenation to MA and the results are displayed in Fig. 5**(D)** and supplementary Table S7. The CZ@Si/NFER with a nominal Cu/Zn ratio of 7/3 (its real molar ratio of 2.43) as confirmed by XRF analysis (supplementary Table S8) revealed a higher MA selectivity of 50.8% compared to other CZ@Si with different Cu/Zn ratios with the MA selectivity of 43.3 – 49.6%, which were attributed to the smaller formations of C_1 and C_{2+} hydrocarbons (26.0%) and methanol (corresponding to the smaller amount of surface water) and an appropriate RWGS reaction activity. To further decrease the hydrocarbon selectivity on the CZ@Si/NFER, the reaction temperature was decreased to 250 °C and main products were found to be methanol and DME without MA formation at a lower CO_2 conversion of 7.1% and hydrocarbon selectivity of 2.7% (methanol/DME selectivity with the respective value of 62.4 and 34.7%) as summarized in supplementary Table S9. Although the reaction temperature of 250 °C was proper for CO_2 hydrogenation and successive DME carbonylation [16,27,33,34], the competitive water adsorption on the active Brønsted acid sites of the NFER surfaces seems to suppress methanol dehydration and its carbonylation activity at lower temperature, which further requires higher reaction temperatures above 300 °C by using the thermally stable core-shell structured CZ@Si catalyst as well.

The different hydrocarbon formations natures and catalytic stability under present tandemly coupled catalytic reaction conditions were verified by cofeeding DME/CO/H_2, and the effects of cofed hydrogen during DME carbonylation itself on the CFER and NFER were investigated and the results are displayed in supplementary Fig. S8 and Table S10. As well-reported in our previous studies [33,34], the nano-sized NFER was found to be excellent for a gas-phase DME carbonylation compared to the commercial CFER, where the higher DME conversion of 21.3% (maximum conversion of 82.4%) and higher MA selectivity of 70.1% (maximum selectivity of 90.2%) were observed on the NFER with very small hydrocarbons less than 1.4% at a steady state. The steady increasing trends of methanol selectivity with time on stream on the CFER and NFER were responsible for the inversely

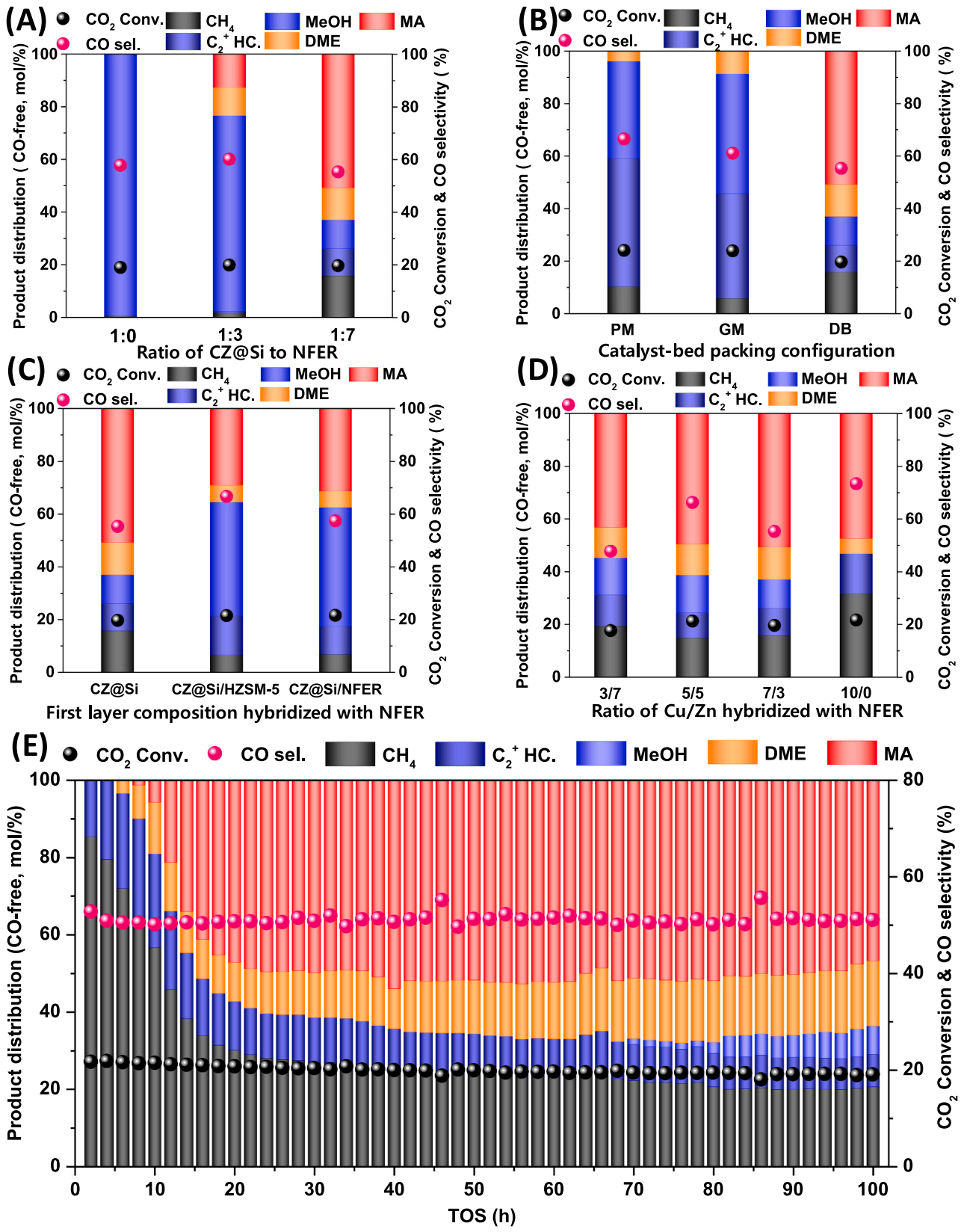

Fig. 5. Catalytic performances on the hybrid CZ@Si/zeolite; **(A)** Effects of different weight ratio of CZ@Si to NFER (1:0, 1:3 and 1:7), **(B)** Effects of different catalyst-bed configuration such as physical powder mixing (PM), granule mixing (GM) and dual bed (DB) manner with CZ@Si and NFER, **(C)** Effects of first layer composition such as bifunctional CZ@Si/HZSM-5 and CZ@Si/NFER (its weight ratio of 2/1) hybridized with NFER in dual bed configuration, **(D)** Effects of Cu/Zn molar ratio of CZ@Si hybridized with NFER and **(E)** Catalytic activity and stability with time on stream (TOS, h) for 100 h on the CZ@Si/NFER (7/3) at T = 300 °C, P = 5.0 MPa, H_2/CO_2 = 3 (4 vol% N_2-balanced) and SV = 625 mL/(g_{cat}·h).

decreasing trend of MA selectivity and DME conversion due to the possible deactivations of active Brønsted acid sites (Fig. S8**(A)** and Fig. S8**(B)**). However, light hydrocarbons selectivity on the NFER (Fig. S8**(C)** and Fig. S8**(D)**) was significantly increased with H_2-containing DME/CO mixed gases during DME carbonylation at similar CO_2 conversions of 21.3 – 23.3%, where the product distributions were largely shifted to light hydrocarbons with a lower MA selectivity since the H_2 can possibly hydrogenate surface methoxy or acetyl species to CH_4 and other hydrocarbons through hydrogen transfer reactions during DME carbonylation reaction [43,44]. The excess amount of H_2 in a feed gas such as DME/CO/H_2/N_2 = 1.5/30.2/62.8/5.5 further enhanced the hydrocarbons formations up to 62.9% (33.4% at steady state) with a steady decrease of MA selectivity with time on stream.

Therefore, for the tandemly coupled reaction conditions such as the direct MA synthesis by CO_2 hydrogenation, the surface intermediates formed on the CZ@Si/NFER can be further reacted to form hydrocarbons by the competitive reactions such as methanol to hydrocarbons through hydrogen transfer reaction on the active Brønsted acid sites. Eventually, the optimized CZ@Si/NFER showed an excellent catalytic stability for 100 h on stream with stable product distributions as displayed in Fig. 5**(E)**. The initially higher CH_4 selectivity above ~80% was gradually decreased after 10 h on stream and MA selectivity was inversely increased up to ~50%, which was mainly attributed to the surface modifications with the help of the deposited surface coke precursors and hydrogen transfer reaction under H_2-containing feed gas. However, the active Brønsted acid sites in the 8-MR channels of the NFER even under the small carbon depositions were stably preserved to convert DME into surface acetyl intermediates [33]. These observations suggest that the current tandem catalysis to synthesize MA by the successive CO_2 hydrogenation-methanol dehydration-carbonylation of DME on the CZ@Si hybridized with NFER zeolite can be realized by introducing the thermally stable metal oxides with highly active and hydrophilic nano-structured FER zeolite structures.

3.4. Surface intermediates and proposed reaction mechanisms

The reaction mechanisms for the tandemly coupled catalytic reaction on the hybridized CZ@Si/NFER were further verified by using in-situ DRIFTS analysis by elucidating reaction intermediates during CO_2 hydrogenation over CZ@Si catalyst as well as carbonylation of DME over NFER zeolite at 0.1 MPa and 300 °C (supplementary Fig. S9). As displayed in Fig. 6**(A-1)**, the absorption peaks located at 2847, 2900, 2943, 2952, 2970 and 2990 cm^{-1} were attributed to C-H vibration modes from surface formate species [45–49]. The increased peak intensity of 2847 and 2915 cm^{-1} by increasing adsorption temperatures (from 50 to 300 °C) and its durations (from 1 to 60 minutes) under CO_2 hydrogenation was mainly originated from C-H vibration modes of surface methoxy species [50–52], which suggests that the methanol formation mechanisms over the CZ@Si seem to follow the well-known formate pathway [53]. As shown in Fig. 6**(A-2)**, the absorption peak located at 2132 cm^{-1} above 250 °C can be assigned to the absorbed CO species on the metallic Cu sites in the Cu-O-Si interfaces [28,54–56], which can be generated from the decomposition of the surface formate species over CZ@Si [57–59] and the absorption peaks located at 2303, 2348 and 2379 cm^{-1} with their similar peak intensity can be also attributed to the presence of gaseous CO_2 [59–61]. These observations strongly suggest that CO_2 hydrogenation activity to form methanol was significantly competitive to the endothermic RWGS reaction to form CO species above 250 °C, where the formations of methanol by CO_2 hydrogenation proceeded through formate pathway by simultaneously forming the adsorbed CO molecules as well. In addition, light hydrocarbons (methane and C_{2+}) formations form surface intermediates by methanol-to-hydrocarbon (MTH) or dimethyl ether-to-hydrocarbon (DTH) reaction seem to be more thermodynamically feasible with the presence of hydrogen at higher temperatures compared to carbonylation reaction as displayed in supplementary Fig. S1. It is also well-known that the surface methoxy species can be an initial intermediate during DME activation step for the further hydrocarbon-pool formation [62] and

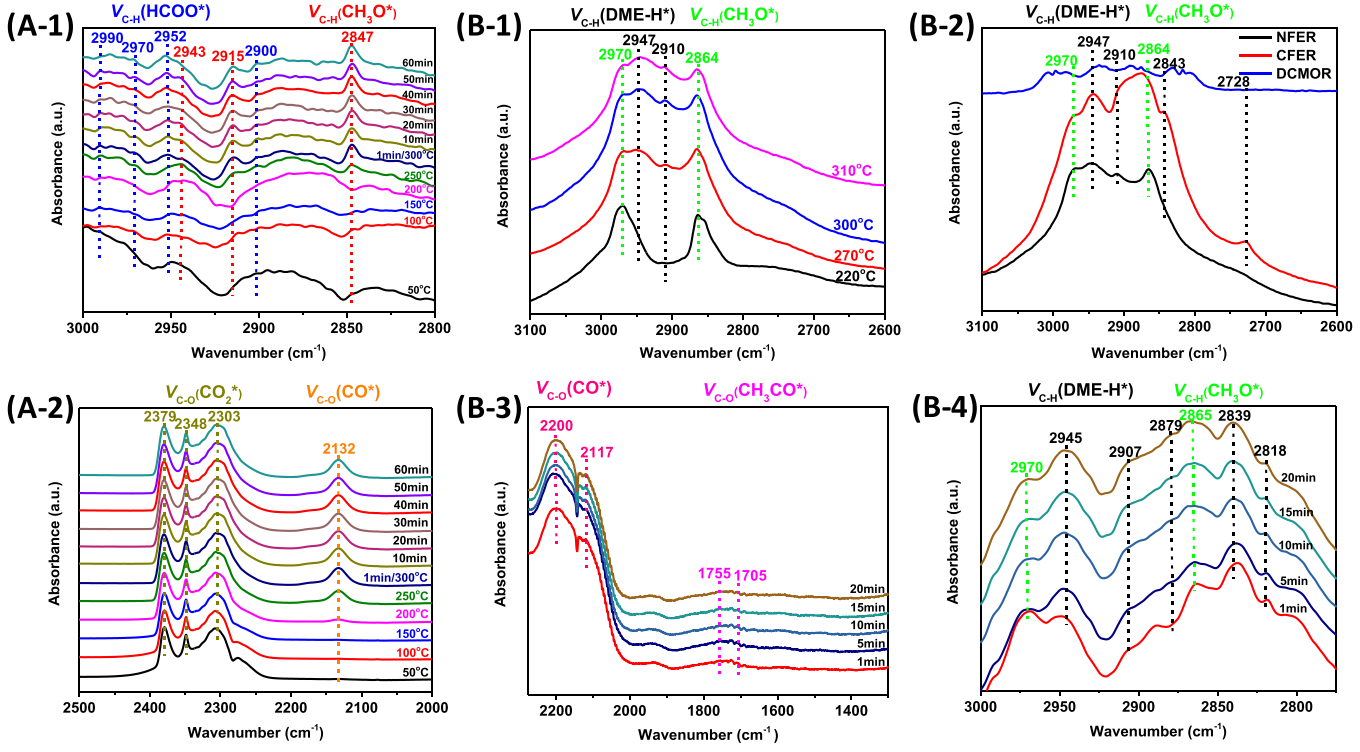

Fig. 6. (A-1) and **(A-2)** Spectra of in-situ DRIFTS on the CZ@Si under CO_2/H_2 (molar ratio of 1/3) feed at 0.1 MPa and 50–300 °C and two different wavenumber, and in-situ DRIFTS spectra for **(B-1)** DME adsorption at different temperatures over NFER itself, **(B-2)** DME adsorption at 300 °C over different zeolites such as NFER, CFER and DCMOR, **(B-3)** and **(B-4)** in-situ DRIFTS spectra under a flow of DME/CO/N_2 (4.47/90.1/5.43, mol%) mixed gas at P = 0.1 MPa and T = 300 °C.

carbonylation reaction as well [19,63].

As displayed in Fig. 6**(B-1)**, the adsorbed DME molecules on the NFER surfaces were firstly dissociated into surface methoxy intermediates as confirmed by the observations of the characteristic C-H vibration modes appeared at 2864 and 2970 cm^{-1}, where the peak intensities were gradually decreased with an increase of adsorption temperature from 220 to 310 °C due to an easier dehydration, carbonylation and hydrocarbon formations [62,63]. The newly observed larger absorption peaks at 2864, 2910 and 2947 cm^{-1} at higher temperatures can be assigned to hydrogen-bonded DME molecules on the Brønsted acid sites [63] to form hydrocarbons by MTH or DTH reaction preferentially [64]. In addition, the adsorption of DME at 300 °C on different zeolites such as the NFER, CFER and DCMOR as displayed in Fig. 6**(B-2)** revealed that the dissociation and adsorption of DME on the DCMOR were found to be much abundant due to the excess amount of stronger acidic sites, which selectively produced the heavier hydrocarbons through MTH or DTH reaction as shown in Fig. 3**(F)**. As displayed in Fig. 6**(B-3)** and Fig. 6**(B-4)**, in-situ DRIFTS results under a cofeeding of CO/DME at 300 °C over the NFER showed two characteristic absorption peaks appeared at 1705 and 1755 cm^{-1}, which are assigned to the typical vibration modes of C═O acetyl groups (CH_3CO*) [35,63–66]. Those observations suggest that the surface methoxy species (CH_3*) is transformed into acetyl intermediate through CO insertion to generate MA product on the active Brønsted acid sites locating in the 8-MR channels of the NFER [19,33,34]. With an increase of adsorption times, the surface methoxy intermediates assigned to the absorption peaks at 2865 and 2945 cm^{-1} were increased as confirmed by the increased hydrogen-bonded DME peaks, which suggests that the formation of hydrocarbons as well as carbonylation of DME simultaneously occurred by being affected by CO insertion rate with different deactivation phenomena.

Furthermore, the formations of light hydrocarbons for tandemly coupled reaction were found to be thermodynamically feasible at a relatively higher reaction temperature of 300 °C and under excess hydrogen environment through MTH or DTH reaction. There are several possible mechanisms for CH_4 production such as methanol/DME decomposition and methanol/DME hydrogenolysis [67] as well as formation of C_2^+ hydrocarbons by MTH or DTH reaction, where the surface methyl acetate can be one of the possible candidates for C-C bond formations [68,69]. As displayed in supplementary Fig. S10, in-situ DRIFTS spectra under a flow of CO/DME at 0.1 MPa and 300 °C on the CFER and DCMOR showed the characteristic C═O vibration bands from the surface acetyl groups located at 1755 and 1705 cm^{-1}, which clearly suggests that the formation of MA happens at the very beginning of adsorption (1 minute) and disappeared after 5 minutes due to fast deactivation by coke depositions and hydrocarbons formation at higher temperatures. Furthermore, in-situ DRIFTS spectra under a flow of H_2-containing DME/CO at 0.1 MPa and 300 °C as displayed in supplementary Fig. S11 also showed the much smaller C═O vibration bands from acetyl groups, which also suggest that the formation of MA seems to be less feasible under an excess hydrogen environment as shown in supplementary Table S10. Those smaller peak intensity of acetyl groups compared to C-H vibration peaks from surface methoxy groups (2864 and 2970 cm^{-1}) and hydrogen-bonded DME vibration peak (2946 cm^{-1}) under hydrogen-rich environment further revealed the more facile hydrocarbon formations by H_2-assistant CO_2-to-MA tandemly coupling reaction.

The reaction mechanisms for the proposed tandemly coupled direct CO_2 hydrogenation to MA through successive hydrogenation-dehydration-carbonylation reaction on the hybridized CZ@Si/NFER are schematically summarized in Fig. 7. Firstly, CO_2 hydrogenation on the core-shell structured CZ@Si produced the formate intermediate (HCOO*), which was transformed into methoxy species (CH_3O*) and methanol by formate-pathway of the adsorbed CO_2 molecules. Simultaneously, CO was formed by RWGS reaction through the hydrogenation of formate intermediates. The appropriate molar ratio of CO to DME was found to be crucial for successive carbonylation of DME on the Brønsted

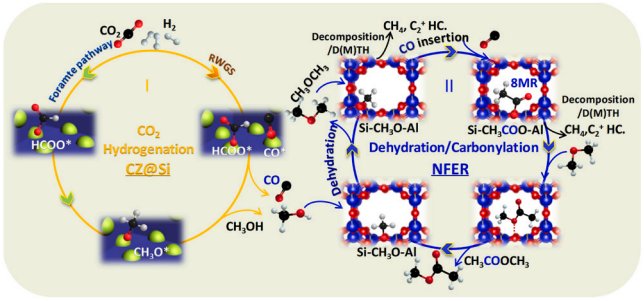

Fig. 7. Proposed reaction mechanisms of the present tandem coupling reactions for a direct MA production by CO_2 hydrogenation to methanol, methanol dehydration to DME and DME carbonylation on the hybridized CZ@Si/NFER catalyst.

acid sites of the NFER zeolite, where DME can be formed by successive dehydration of methanol on the acidic sites of zeolites. Eventually, the DME was transformed into the surface methoxy species and CO insertion occurred in the active Brønsted acid sites located in the 8-MR channels of the FER zeolite to form the acetyl intermediate groups by carbonylation to form MA. The MTH or DTH reaction pathways are responsible for the formations of undesired methane and C_2^+ hydrocarbons from the surface hydrogen-bonded DME or methoxy species under H_2-excess environment on the hybridized CZ@Si/NFER catalyst. In addition, the surface hydrophobicity-enhanced NFER treated with hexadecyl trimethoxy silane according to the previous work [70] showed a slightly increased hydrocarbons selectivity with an excellent stability for 100 h reaction (a little lower CO_2 conversion below ~17% due to the partial blockages of acidic sites as well as easier water removal nature) as displayed in supplementary Fig. S12, which were possibly attributed to the slightly enhanced M/DTH reaction activity with a suppressed CO adsorption capacity on the modified acidic sites of the NFER. Interestingly, the present CZ@Si/NFER still showed a higher MA selectivity compared to other reported catalytic systems through tandemly coupled CO_2 hydrogenation (~20% conversion) and carbonylation reaction to selectively form MA (50.8% selectivity) as summarized in supplementary Table S11. The smaller deactivation rate on the optimized CZ@Si/NFER under the tandemly coupled direct CO_2 hydrogenation to MA was originated from the enhanced CO insertion rate by suppressing MTH or DTH reaction activity on the larger active Brønsted (B) acid sites in the 8-MR channels of the NFER zeolite.

4. Conclusions

Tandemly coupled CO_2 hydrogenation with successive carbonylation to MA reaction was investigated by stepwise catalytic reactions of CO_2-to-methanol (DME)/CO intermediate over CZ@Si catalyst stabilized by forming stable Cu-O-Si interfaces though SiO_2-encapsulation as well as by further doing carbonylation reaction of surface methoxy (CH_3*) species formed from dissociative adsorption of DME/methanol with an enhanced CO insertion over nano-structured NFER zeolite. The higher thermally stable metallic Cu sites (homogeneously distributed and encapsulated Cu-ZnO nanoparticles with its size of ~3 nm stabilized through the well-defined SMSI effects between Cu and SiO_2 shells by forming Cu-O-Si interfaces) were found to be appropriate to in-situ produce a proper CO/methanol ratio to boost up carbonylation rate formed by CO_2 hydrogenation and RWGS reaction to produce MA oxygenate. The superior catalytic activity and stability for direct one-step CO_2 conversion to MA on the CZ@Si/NFER was also attributed to the fast CO insertion rate into the surface methoxy intermediates to form surface acetyl groups with suppressed hydrocarbon formations by D(M)TH reaction over moderate acidity as well as facile intermediate diffusion natures on the nano-structured FER zeolite. In-situ DRIFTS analysis and thermodynamic considerations suggested that CO_2 and H_2 reactant

were firstly converted into methanol/CO through formate-pathway, which was dehydrated to form DME, and DME carbonylation was carried out on the Brønsted acid sites in the 8-MR channels of the NFER to form MA product. The present tandemly coupled catalytic system suggests the novel catalytic system to realize direct CO_2 hydrogenation to oxygenate formation by successive dehydration and carbonylation to form MA on the optimal hybridized CZ@Si/NFER by suppressing the formations of hydrocarbons and surface coke precursors.

CRediT authorship contribution statement

Bae Jong Wook: Writing – review & editing, Supervision, Conceptualization. **Wang Xu:** Writing – original draft, Investigation, Formal analysis. **Jeong So Yun:** Formal analysis, Data curation. **Jung Hyun Seung:** Methodology, Investigation.

Declaration of Competing Interest

The authors declare that they have no known competing financial interests or personal relationships that could have appeared to influence the work reported in this paper.

Data availability

Data will be made available on request.

Acknowledgements

The authors would sincerely like to acknowledge the financial support from the National Research Foundation of Korea (NRF) grant funded by the South Korea government (NRF-2021R1A4A1024129 and NRF-2022M3J2A1085553). This work was also supported by the Carbon Neutral Industrial Strategic Technology Development Program funded by the Ministry of Trade, Industry & Energy (MOTIE) of the Republic of Korea (RS-2023-00261088).

Appendix A. Supporting information

Supplementary data associated with this article can be found in the online version at doi:10.1016/j.apcatb.2024.123829.

References

[1] C. Zhu, J. Liu, M.B. Li, J.E. Bäckvall, Palladium-catalyzed oxidative dehydrogenative carbonylation reactions using carbon monoxide and mechanistic overviews, Chem. Soc. Rev. 49 (2) (2020) 341–353.
[2] X.F. Wu, X. Fang, L. Wu, R. Jackstell, H. Neumann, M. Beller, Transition-metal-catalyzed carbonylation reactions of olefins and alkynes: a personal account, Acc. Chem. Res. 47 (4) (2014) 1041–1053.
[3] K. Dong, X.F. Wu, Carbonylations with CO_2 as the CO source and reactivity modifier, Angew. Chem. Int. Ed. 56 (20) (2017) 5399–5401.
[4] S. Fu, S. Yao, S. Guo, G.C. Guo, W. Yuan, T.B. Lu, Z.M. Zhang, Feeding carbonylation with CO_2 via the synergy of single-site/nanocluster catalysts in a photosensitizing MOF, J. Am. Chem. Soc. 143 (49) (2021) 20792–20801.
[5] Q. Qian, J. Zhang, M. Cui, B. Han, Synthesis of acetic acid via methanol hydrocarboxylation with CO_2 and H_2, Nat. Commun. 7 (1) (2016) 11481.
[6] Y. Wang, Q. Qian, J. Zhang, B.B.A. Bediako, Z. Wang, H. Liu, B. Han, Synthesis of higher carboxylic acids from ethers, CO_2 and H_2, Nat. Commun. 10 (1) (2019) 5395.
[7] B.B. Asare Bediako, Q. Qian, B. Han, Synthesis of C_{2+} chemicals from CO_2 and H_2 via C–C bond formation, Acc. Chem. Res. 54 (10) (2021) 2467–2476.
[8] D.U. Nielsen, X.M. Hu, K. Daasbjerg, T. Skrydstrup, Chemically and electrochemically catalysed conversion of CO_2 to CO with follow-up utilization to value-added chemicals, Nat. Catal. 1 (4) (2018) 244–254.
[9] Y.S. Xia, M. Tang, L. Zhang, J. Liu, C. Jiang, G.K. Gao, L.K. Dong, Y.Q. Lan, Tandem utilization of CO_2 photoreduction products for the carbonylation of aryl iodides, Nat. Commun. 13 (1) (2022) 2964.
[10] R. Sang, Y. Hu, R. Razzaq, G. Mollaert, H. Atia, U. Bentrup, M. Sharif, H. Neumann, H. Junge, R. Jackstell, B.U.W. Maes, M. Beller, A practical concept for catalytic carbonylations using carbon dioxide, Nat. Commun. 13 (1) (2022) 4432.
[11] M.T. Jensen, M.H. Rønne, A.K. Ravn, R.W. Juhl, D.U. Nielsen, X.M. Hu, S. U. Pedersen, K. Daasbjerg, T. Skrydstrup, Scalable carbon dioxide electroreduction coupled to carbonylation chemistry, Nat. Commun. 8 (1) (2017) 489.
[12] M.D. Porosoff, B. Yan, J.G. Chen, Catalytic reduction of CO_2 by H_2 for synthesis of CO, methanol and hydrocarbons: challenges and opportunities, Energy Environ. Sci. 9 (1) (2016) 62–73.
[13] Y. Wang, S. Kattel, W. Gao, K. Li, P. Liu, J.G. Chen, H. Wang, Exploring the ternary interactions in Cu–ZnO–ZrO_2 catalysts for efficient CO_2 hydrogenation to methanol, Nat. Commun. 10 (1) (2019) 1166.
[14] E.L. Kunkes, F. Studt, F. Abild-Pedersen, R. Schlögl, M. Behrens, Hydrogenation of CO_2 to methanol and CO on Cu/ZnO/Al_2O_3: is there a common intermediate or not? J. Catal. 328 (2015) 43–48.
[15] Q. Sun, N. Wang, J. Yu, Advances in catalytic applications of zeolite-supported metal catalysts, Adv. Mater. 33 (2021) 2104442.
[16] H. Ham, S.W. Baek, C.H. Shin, J.W. Bae, Roles of structural promoters for direct CO_2 hydrogenation to dimethyl ether over ordered mesoporous bifunctional Cu/M–Al_2O_3 (M = Ga or Zn), ACS Catal. 9 (1) (2018) 679–690.
[17] R. Ye, J. Ding, W. Gong, M.D. Argyle, Q. Zhong, Y. Wang, C.K. Russell, Z. Xu, A. G. Russell, Q. Li, M. Fan, Y.G. Y, CO_2 hydrogenation to high-value products via heterogeneous catalysis, Nat. Commun. 10 (1) (2019) 5698.
[18] Y. Liu, K. Murata, M. Inaba, I. Takahara, Synthesis of ethanol from methanol and syngas through an indirect route containing methanol dehydrogenation, DME carbonylation, and methyl acetate hydrogenolysis, Fuel Process. Technol. 110 (2013) 206–213.
[19] E. Zhan, Z. Xiong, W. Shen, Dimethyl ether carbonylation over zeolites, J. Energy Chem. 36 (2019) 51–63 (a);
H.S. Jung, B.G. Kim, J.W. Bae, Synthetic routes of clean hydrocarbons fuels and oxygenates by catalytic conversions of carbon oxides, Appl. Catal. B: Environ. 343 (2024) 123477 (b).
[20] Y. Zhang, Q. Sun, J. Deng, D. Wu, S. Chen, A high activity Cu/ZnO/Al_2O_3 catalyst for methanol synthesis: Preparation and catalytic properties, Appl. Catal. A: Gen. 158 (1-2) (1997) 105–120.
[21] J. Wang, G. Li, Z. Li, C. Tang, Z. Feng, H. An, H. Liu, T. Liu, C. Li, A highly selective and stable ZnO-ZrO_2 solid solution catalyst for CO_2 hydrogenation to methanol, Sci. Adv. 3 (10) (2017) e1701290.
[22] J. Wang, C. Tang, G. Li, Z. Han, Z. Li, H. Liu, F. Cheng, C. Li, High-performance $MaZrO_x$ (Ma = Cd, Ga) solid-solution catalysts for CO_2 hydrogenation to methanol, ACS Catal. 9 (11) (2019) 10253–10259.
[23] M.S. Frei, M. Capdevila-Cortada, R. García-Muelas, C. Mondelli, N. López, J. A. Stewart, D.C. Ferré, J. Pérez-Ramírez, Mechanism and microkinetics of methanol synthesis via CO_2 hydrogenation on indium oxide, J. Catal. 361 (2018) 313–321.
[24] A. Tsoukalou, P.M. Abdala, D. Stoian, X. Huang, M.G. Willinger, A. Fedorov, C. R. Müller, Structural evolution and dynamics of an In_2O_3 catalyst for CO_2 hydrogenation to methanol: an operando XAS-XRD and in situ TEM study, J. Am. Chem. Soc. 141 (34) (2019) 13497–13505.
[25] O. Martin, A.J. Martín, C. Mondelli, S. Mitchell, T.F. Segawa, R. Hauert, C. Drouilly, D. Curulla-Ferré, J. Pérez-Ramírez, J. Pérez-Ramírez, Indium oxide as a superior catalyst for methanol synthesis by CO_2 hydrogenation, Angew. Chem. Int. Ed. 55 (21) (2016) 6261–6265.
[26] K. Lee, U. Anjum, T.P. Araújo, C. Mondelli, Q. He, S. Furukawa, J. Pérez-Ramírez, S.M. Kozlov, N. Yan, Atomic Pd-promoted $ZnZrO_x$ solid solution catalyst for CO_2 hydrogenation to methanol, Appl. Catal. B: Environ. 304 (2022) 120994.
[27] (a) X. Wang, S.Y. Jeong, H.S. Jung, D. Shen, M. Ali, F. Zafar, C.H. Chung, J.W. Bae, Catalytic activity for direct CO_2 hydrogenation to dimethyl ether with different proximity of bifunctional Cu-ZnO-Al_2O_3 and ferrierite, Appl. Catal. B: Environ. 327 (2023) 122456;
(b) F. Zafar, R. Zhao, M. Ali, Y.M. Park, H.S. Roh, X. Gao, J. Tian, J.W. Bae, Unprecedented contributions of In_2O_3 promoter on ordered mesoporous Cu/Al_2O_3 for CO_2 hydrogenation to oxygenates, Chem. Eng. J. 439 (2022) 135649.
[28] S. Wang, K. Feng, D. Zhang, D. Yang, M. Xiao, C. Zhang, L. He, B. Yan, G.A. Ozin, W. Sun, Stable Cu catalysts supported by two-dimensional SiO_2 with strong metal-support interaction, Adv. Sci. 9 (9) (2022) 2104972.
[29] P. Cheung, A. Bhan, G.J. Sunley, E. Iglesia, Selective carbonylation of dimethyl ether to methyl acetate catalyzed by acidic zeolites, Angew. Chem. Int. Ed. 45 (10) (2006) 1617–1620.
[30] J. Yao, X. Feng, J. Fan, Y. He, R. Kosol, Y. Zeng, G. Liu, Q. Ma, G. Yang, N. Tsubaki, Effects of mordenite zeolite catalyst synthesis conditions on dimethyl ether carbonylation, Micropor. Mesopor. Mater. 306 (2020) 110431.
[31] Q. Wei, G. Yang, X. Gao, L. Tan, P. Ai, P. Zhang, P. Lu, Y. Yoneyama, N. Tsubaki, A facile ethanol fuel synthesis from dimethyl ether and syngas over tandem combination of Cu-doped HZSM35 with Cu-Zn-Al catalyst, Chem. Eng. J. 316 (2017) 832–841.
[32] Y. Li, S. Huang, Z. Cheng, K. Cai, L. Li, E. Milan, J. Lv, Y. Wang, Q. Sun, X. Ma, Promoting the activity of Ce-incorporated MOR in dimethyl ether carbonylation through tailoring the distribution of Brønsted acids, Appl. Catal. B: Environ. 256 (2019) 117777.
[33] H. Ham, H.S. Jung, H.S. Kim, J. Kim, S.J. Cho, W.B. Lee, M.J. Park, J.W. Bae, Gas-phase carbonylation of dimethyl ether on the stable seed-derived ferrierite, ACS Catal. 10 (9) (2020) 5135–5146.
[34] S.Y. Park, C.H. Shin, J.W. Bae, Selective carbonylation of dimethyl ether to methyl acetate on Ferrierite, Catal. Commun. 75 (2016) 28–31.
[35] P. Cheung, A. Bhan, G.J. Sunley, D.J. Law, E. Iglesia, Site requirements and elementary steps in dimethyl ether carbonylation catalyzed by acidic zeolites, J. Catal. 245 (1) (2007) 110–123.
[36] A. Ramirez, X. Gong, M. Caglayan, S.A.F. Nastase, E. Abou-Hamad, L. Gevers, L. Cavallo, A.D. Chowdhury, J. Gascon, Selectivity descriptors for the direct hydrogenation of CO_2 to hydrocarbons during zeolite-mediated bifunctional catalysis, Nat. Commun. 12 (1) (2021) 1–13.

[37] Y. Wang, G. Wang, L.I. van der Wal, K. Cheng, Q. Zhang, K.P. de Jong, Y. Wang, Visualizing element migration over bifunctional metal-zeolite catalysts and its impact on catalysis, Angew. Chem. Int. Ed. 60 (32) (2021) 17735–17743.
[38] F. Jiao, J. Li, X. Pan, J. Xiao, H. Li, H. Ma, M. Wei, Y. Pan, Z. Zhou, M. Li, S. Miao, J. Li, Y. Zhu, D. Xiao, T. He, J. Yang, F. Qi, Q. Fu, X. Bao, Selective conversion of syngas to light olefins, Science 351 (6277) (2016) 1065–1068.
[39] J. Wei, Q. Ge, R. Yao, Z. Wen, C. Fang, L. Guo, J. Sun, Directly converting CO_2 into a gasoline fuel, Nat. Commun. 8 (1) (2017) 15174.
[40] P. Gao, S. Li, X. Bu, S. Dang, Z. Liu, H. Wang, Y. Sun, Direct conversion of CO_2 into liquid fuels with high selectivity over a bifunctional catalyst, Nat. Chem. 9 (10) (2017) 1019–1024.
[41] S. Kasipandi, J.W. Bae, Recent advances in direct synthesis of value-added aromatic chemicals from syngas by cascade reactions over bifunctional catalysts, Adv. Mater. 31 (2019) 1803390.
[42] H. Jiang, Z. Hou, Y. Luo, A kinetic view on proximity-dependent selectivity of carbon dioxide reduction on bifunctional catalysts, ACS Catal. 10 (22) (2020) 13518–13523.
[43] S.S. Arora, D.L. Nieskens, A. Malek, A. Bhan, Lifetime improvement in methanol-to-olefins catalysis over chabazite materials by high-pressure H_2 co-feeds, Nat. Catal. 1 (9) (2018) 666–672.
[44] X. Zhao, J. Li, P. Tian, L. Wang, X. Li, S. Lin, X. Guo, Z. Liu, Achieving a superlong lifetime in the zeolite-catalyzed MTO reaction under high pressure: synergistic effect of hydrogen and water, ACS Catal. 9 (4) (2019) 3017–3025.
[45] M. Marwood, R. Doepper, A. Renken, In-situ surface and gas phase analysis for kinetic studies under transient conditions: The catalytic hydrogenation of CO_2, Appl. Catal. A: Gen. 151 (1) (1997) 223–246.
[46] P. Sripada, J. Kimpton, A. Barlow, T. Williams, S. Kandasamy, S. Bhattacharya, Investigating the dynamic structural changes on Cu/CeO_2 catalysts observed during CO_2 hydrogenation, J. Catal. 381 (2020) 415–426.
[47] A.S. Malik, S.F. Zaman, A.A. Al-Zahrani, M.A. Daous, H. Driss, L.A. Petrov, Selective hydrogenation of CO_2 to CH_3OH and in-depth DRIFT analysis for $PdZn/ZrO_2$ and $CaPdZn/ZrO_2$ catalysts, Catal. Today 357 (2020) 573–582.
[48] P. Hongmanorom, J. Ashok, P. Chirawatkul, Z. Kawi, Interfacial synergistic catalysis over Ni nanoparticles encapsulated in mesoporous ceria for CO_2 methanation, Appl. Catal. B: Environ. 297 (2021) 120454.
[49] J.C. Medina, M. Figueroa, R. Manrique, J.R. Pereira, P.D. Srinivasan, J.J. Bravo-Suárez, V.G.B. Medrano, R. Jiménez, A. Karelovic, Catalytic consequences of Ga promotion on Cu for CO_2 hydrogenation to methanol, Catal. Sci. Technol. 7 (15) (2017) 3375–3387.
[50] C. Wang, T. Lin, X. Qi, F. Yu, Y. Lu, L. Zhong, Y. Sun, Direct conversion of syngas to higher alcohols over multifunctional catalyst: the role of copper-based component and catalytic mechanism, J. Phys. Chem. C 125 (11) (2021) 6137–6146.
[51] D.G. Araiza, A. Gómez-Cortés, G. Díaz, Reactivity of methanol over copper supported on well-shaped CeO_2: a TPD-DRIFTS study, Catal. Sci. Technol. 7 (22) (2017) 5224–5235.
[52] P. Jia, Y. Liu, R. Yang, P. Luo, W. Huang, Insight into the structural sensitivity of CuZnAl catalysts for CO hydrogenation to alcohols, Fuel 323 (2022) 124265.
[53] S. Kattel, B. Yan, Y. Yang, J.G. Chen, P. Liu, Optimizing binding energies of key intermediates for CO_2 hydrogenation to methanol over oxide-supported copper, J. Am. Chem. Soc. 138 (38) (2016) 12440–12450.
[54] T. Pu, W. Zhang, M. Zhu, Engineering heterogeneous catalysis with strong metal–support interactions: characterization, theory and manipulation, Angew. Chem. Int. Ed. 62 (4) (2023) e202212278.
[55] Y. Jiang, H. Yang, P. Gao, X. Li, J. Zhang, H. Liu, H. Wang, Y. Sun, Slurry methanol synthesis from CO_2 hydrogenation over micro-spherical SiO_2 support Cu/ZnO, Catal., J. CO_2 Util. 26 (2018) 642–651.
[56] Z. Zhang, X. Chen, J. Kang, Z. Yu, J. Tian, Z. Gong, A. Jia, R. You, K. Qian, S. He, B. Teng, Y. Cui, Y. Wang, W. Zhang, W. Huang, The active sites of Cu-ZnO catalysts for water gas shift and CO hydrogenation reactions, Nat. Commun. 12 (1) (2021) 4331.
[57] E. Pahija, C. Panaritis, S. Gusarov, J. Shadbahr, F. Bensebaa, G. Patience, D. C. Boffito, Experimental and computational synergistic design of Cu and Fe catalysts for the reverse water-gas shift: a review, ACS Catal. 12 (12) (2022) 6887–6905.
[58] A.M. Bahmanpour, F. Héroguel, M. Kılıç, C.J. Baranowski, L. Artiglia, U. Röthlisberger, J.S. Luterbacher, O. Kröcher, Cu–Al spinel as a highly active and stable catalyst for the reverse water gas shift reaction, ACS Catal. 9 (7) (2019) 6243–6251.
[59] K. Zhao, L. Wang, M. Calizzi, E. Moioli, A. Züttel, In situ control of the adsorption species in CO_2 hydrogenation: determination of intermediates and byproducts, J. Phys. Chem. C. 122 (36) (2018) 20888–20893.
[60] R. Liu, D. Leshchev, E. Stavitski, M. Juneau, J.N. Agwara, M.D. Porosoff, Selective hydrogenation of CO_2 and CO over potassium promoted Co/ZSM-5, Appl. Catal. B: Environ. 284 (2021) 119787.
[61] X. Wang, H. Shi, J. Szanyi, Controlling selectivities in CO_2 reduction through mechanistic understanding, Nat. Commun. 8 (1) (2017) 513.
[62] (a) T.R. Forester, R.F. Howe, In situ FTIR studies of methanol and dimethyl ether in ZSM-5, J. Am. Chem. Soc. 109 (17) (1987) 5076–5082;
(b) A. Hwang, A. Bhan, Deactivation of zeolites and zeotypes in methanol-to-hydrocarbons catalysis: mechanisms and circumvention, Acc. Chem. Res. 52 (9) (2019) 2647–2656.
[63] H. Zhou, W. Zhu, L. Shi, H. Liu, S. Liu, Y. Ni, Y. Liu, Y. He, S. Xu, L. Li, Z. Liu, In situ DRIFT study of dimethyl ether carbonylation to methyl acetate on H-mordenite, J. Mol. Catal. A: Chem. 417 (2016) 1–9.
[64] J. Li, Z. Wei, Y. Chen, B. Jing, Y. He, M. Dong, H. Jiao, X. Li, Z. Qin, J. Wang, W. Fan, A route to form initial hydrocarbon pool species in methanol conversion to olefins over zeolites, J. Catal. 317 (2014) 277–283.
[65] O. Kresnawahjuesa, R.J. Gorte, D. White, Characterization of acylating intermediates formed on H-ZSM-5, J. Mol. Catal. A: Chem. 208 (1-2) (2004) 175–185.
[66] X. Feng, J. Yao, H. Li, Y. Fang, Y. Yoneyama, G. Yang, N. Tsubaki, A brand new zeolite catalyst for carbonylation reaction, Chem. Commun. 55 (8) (2019) 1048–1051.
[67] W. Zhao, B. Zhang, G. Wang, H. Guo, Methane formation route in the conversion of methanol to hydrocarbons, J. Energy Chem. 23 (2) (2014) 201–206.
[68] A.D. Chowdhury, A.L. Paioni, K. Houben, G.T. Whiting, M. Baldus, B. M. Weckhuysen, Bridging the gap between the direct and hydrocarbon pool mechanisms of the methanol-to-hydrocarbons process, Angew. Chem. Int. Ed. 57 (27) (2018) 8095–8099.
[69] P.N. Plessow, F. Studt, Unraveling the mechanism of the initiation reaction of the methanol to olefins process using ab initio and DFT calculations, ACS Catal. 7 (11) (2017) 7987–7994.
[70] Z. Jin, L. Wang, E. Zuidema, K. Mondal, M. Zhang, J. Zhang, C. Wang, X. Meng, H. Yang, C. Mesters, F.S. Xiao, Hydrophobic zeolite modification for in situ peroxide formation in methane oxidation to methanol, Science 367 (2020) 193–197.